Interferometric coherence optimization

using the polarimetric signatures

Boularbah Souissi, Mounira Ouarzeddine, Aichouche Belhadj-Aissa
Department of telecommunication
Faculty of Electronics and Computing, USTHB university
Algiers, Algeria
m.ouarzeddine@yahoo.fr

***Abstract*— The coherence optimization based on the eigenvalues in radar polarimetry is used to enhance the quality of SAR interferograms. A second and an alternative coherence optimization algorithm which consists in looking at the possible coherence for every combination of elliptical polarizations extracted from the polarimetric signatures and selecting the highest one is also developed, tested and compared with the coherence optimization method. It is shown that, the coherence algorithm based on polarimetric signature performs better than the 1st approach but it takes a longer execution time. SAR images used have been acquired at P-band over the forest of Tapajos in Brazil.**

Keywords-component; interferometry; polarimetry; optimization;interferogram

I. INTRODUCTION (HEADING 1)

Polarimetry SAR is concerned with the extraction of the target properties from the behavior of scattered (reflected) waves from a target such as the textural fine-structure, target orientation and shape, symmetries and material constituents [1]. The polarimetric response is highly sensitive to the scattering mechanism of a pixel, so that PolSAR sorts and identifies radar targets. Whereas, SAR interferometry (InSAR) has been established as a technique in order to generate topographic maps or digital elevation models (DEM) from the phase difference between two coherent SAR images called interferogram [2]. Interferometric data can be acquired simultaneously in a Single-Pass mode, by using two antennas on the same platform or in a Repeat-Pass (multi pass)-Mode over the same area at different times [3]. The first method is applicable only to airborne SAR systems or space shuttles, while the second method is most suited to spaceborne SAR systems. Repeat-pass interferometry requires only one antenna and a precise location of the flight path. The information derived from these interferometric data sets besides to the topography can be used to measure several geophysical quantities, such as deformations (volcanoes, earthquakes), glacier flows, ocean currents, vegetation parameters, etc.

Polarimetric interferometry known as PolInSAR combines both SAR polarimetry and SAR interferometry [1][3]. It has become a popular area for research in the remote sensing field. The PolInSAR is an extension of conventional interferometry where full-polarization information is gathered at either end of the interferometric baseline. The method is most usefully applied to targets that exhibit volume scattering, such as forests, where the results from conventional interferometry become ambiguous. In this paper, we review the technology and the theoretical aspects signal of InSAR and discuss and assess by using mathematical formulations, the impact of radar polarimetry on the optimization of the interferometric coherence.

The PolInSAR technique helps to retrieve the dominant scattering targets and isolate the effective scattering centers in the same time [4]. In this way, a coherence optimization method based on the eigenvlaue values and eigenvectors is used to enhance the quality of SAR interferograms. We propose also a second and an alternative coherence optimization algorithm which consists in looking at the possible coherence for every combination of elliptical polarizations extracted from the polarimetric signatures and selecting the highest one is also developed, tested and compared with the coherence optimization method.

II. POLARIMETRIC SAR INTERFEROETRY

With the introduction of polarimetric SAR interferometry a coherence optimization technique was developed by Cloud and Papathanassious [3]. It is considered the most general one, since it allows different polarization states at the two baseline ends to estimate the dominant scattering mechanisms and their interferometric phases. The starting point is the definition of the pauli target vector for both ends of the baseline, $\vec{k}_{p1}$ and $\vec{k}_{p2}$ given by:

$$\overrightarrow{k_{p1}} = \frac{1}{\sqrt{2}}\left[S_{hh1} + S_{vv1} \quad S_{hh1} - S_{vv1} \quad \sqrt{2}S_{hv1}\right]^T \quad (1)$$

$$\overrightarrow{k_{p2}} = \frac{1}{\sqrt{2}}\left[S_{hh2} + S_{vv2} \quad S_{hh2} - S_{vv2} \quad \sqrt{2}S_{hv2}\right]^T \quad (2)$$

Stacking the scattering vectors $\overrightarrow{k_{p1}}$ and $\overrightarrow{k_{p2}}$ one over the other, we generate a six-dimensional vector. We use the outer product formed from this six-dimentional vector to define a 6x6 hermitian positive semidefinite matrix $[T_6]$:

$$[T_6] = \left\langle \begin{bmatrix} \overrightarrow{k_{p1}} \\ \overrightarrow{k_{p2}} \end{bmatrix} \begin{bmatrix} \overrightarrow{k_{p1}}^{*T} & \overrightarrow{k_{p2}}^{*T} \end{bmatrix} \right\rangle = \begin{bmatrix} [T_{11}] & [\Omega_{12}] \\ [\Omega_{12}]^{*T} & [T_{22}] \end{bmatrix} \quad (3)$$

The complete information measured by the SAR system can be represented in form of three 3x3 complex matrices $[T_{11}] = \langle \overrightarrow{k_{p1}}\, \overrightarrow{k_{p1}}^{*T} \rangle$, $[T_{22}] = \langle \overrightarrow{k_{p2}}\, \overrightarrow{k_{p2}}^{*T} \rangle$ and $[\Omega_{12}] = \langle \overrightarrow{k_{p1}}\, \overrightarrow{k_{p2}}^{*T} \rangle$. $[T_{11}]$ and $[T_{22}]$ are the conventional hermitian coherency matrices which describe the polarimetric properties for each image separately. However, $[\Omega_{12}]$ is a new 3x3 complex matrix which contains not only polarimetric information but also the interferometric phase relations of the different polarimetric channels between both images.

A. *Complex coherence*

Introducing two unitary complex vectors $\overrightarrow{\omega_1}$ and $\overrightarrow{\omega_2}$, which may be interpreted as generalized scattering mechanisms, we are able to generate two complex scalar images by projecting the scattering vectors onto $\overrightarrow{k_{p1}}$ and $\overrightarrow{k_{p2}}$, respectively, as:

$$i_1 = \overrightarrow{\omega_1}^{*T} \overrightarrow{k_{p1}} \text{ and } i_2 = \overrightarrow{\omega_2}^{*T} \overrightarrow{k_{p2}} \tag{4}$$

A general expression for the complex interferometric coherence for an arbitrary choice of scattering mechanisms $\overrightarrow{\omega_1}$ and $\overrightarrow{\omega_2}$ may be derived as:

$$\check{\gamma} = \frac{\langle \overrightarrow{\omega_1}^{*T} [\Omega_{12}] \overrightarrow{\omega_2} \rangle}{\sqrt{\langle \overrightarrow{\omega_1}^{*T} [T_{11}] \overrightarrow{\omega_1} \rangle \langle \overrightarrow{\omega_2}^{*T} [T_{22}] \overrightarrow{\omega_2} \rangle}} = \gamma e^{i\phi} \tag{5}$$

Where γ is the amplitude of the complex coherence and ϕ is the desired interferogram. According to (4), each image corresponds, to a projection of the scattering vector $\vec{k}$ from each resolution cell in the image onto the vector $\vec{\omega}$ ($i = \vec{\omega}^{*T} \vec{k}$) . The interferometric phase of three interferograms can be formed by using different linear combinations of elements of the scattering vectors in the linear basis. The corresponding interferograms can be considered to be formed by the use of $hh_1 hh_2^*$ interferogram, $\overrightarrow{\omega_1} = \overrightarrow{\omega_2} = [1/\sqrt{2} \quad -1/\sqrt{2} \quad 0]^T$, for $hv_1 hv_2^*$ interferogram $\overrightarrow{\omega_1} = \overrightarrow{\omega_2} = [0 \quad 0 \quad 1]^T$ and for $vv_1 vv_2^*$ interferogram $\overrightarrow{\omega_1} = \overrightarrow{\omega_2} = [1/\sqrt{2} \quad 1/\sqrt{2} \quad 0]^T$. Fig. 1 shows the coherence and the interferogram of $hh_1 hh_2^*$.

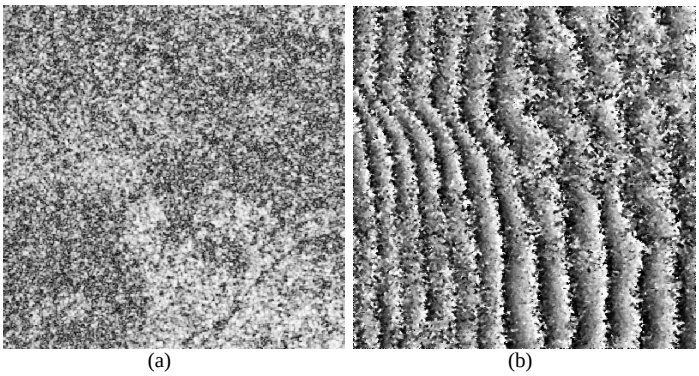

(a) (b)

Figure 1. Coherence and interferogram of HH1-HH2

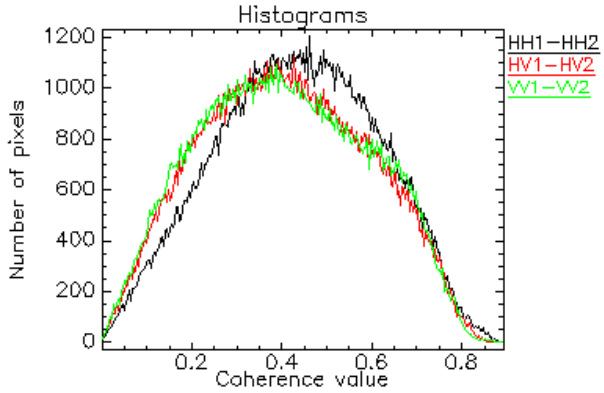

Figure 2. Coherence histograms: HH1-HH2, VV1-VV2, and HV1-HV2

A significant loss in coherence is observable in dark regions and is caused by volume decorrelation resulting from the forested areas. The corresponding histograms shown in Fig. 2 represent a quantitative comparison of the polarization dependent coherence behavior in the three interferograms. The Maximum values are: 0.435 with 1124 pixels for HH1-HH2, 0.409 with 1024 pixels for HV1-HV2 and 0.407 with 1016 pixels for VV1-VV2. By analyzing the results, we note that the coherence represented by HH-HH is the best.

B. *Coherence optimization*

As demonstrated in the previous section, the interferometric coherence has a strong dependency on the polarization states used to form the interferogram. This dependency leads us to consider the question of which linear combinations of polarization states that give the dominant scattering mechanism which yield the highest possible interferometric coherence.

The optimization problem is applied on the general vector formulation of the interferometric coherence as given in (5) by maximizing the complex Lagrangian defined as:

$$L = \overrightarrow{\omega_1}^{*T} [\Omega_{12}] \overrightarrow{\omega_2} + \lambda_1 \left(\overrightarrow{\omega_1}^{*T} [T_{11}] \overrightarrow{\omega_1} - C_1 \right) + \lambda_2 \left(\overrightarrow{\omega_2}^{*T} [T_{22}] \overrightarrow{\omega_2} - C_2 \right) \tag{6}$$

C_1 and C_2 are constants. λ_1 and λ_2 are Lagrange multipliers introduced so that we maximize the numerator of (5) while keeping the denominator constant. After an algebraic simplification, it yields to:

$$[T_{22}]^{-1} [\Omega_{12}]^{*T} [T_{11}]^{-1} [\Omega_{12}] \overrightarrow{\omega_2} = \nu \overrightarrow{\omega_2} \rightarrow$$

$$[B][A] \overrightarrow{\omega_2} = \nu \overrightarrow{\omega_2} \tag{7}$$

$$[T_{11}]^{-1} [\Omega_{12}] [T_{22}]^{-1} [\Omega_{12}]^{*T} \overrightarrow{\omega_1} = \nu \overrightarrow{\omega_1} \rightarrow$$

$$[A][B] \overrightarrow{\omega_1} = \nu \overrightarrow{\omega_1} \tag{8}$$

Where $[A] = [T_{11}]^{-1} [\Omega_{12}]$ and $[B] = [T_{22}]^{-1} [\Omega_{12}]^{*T}$.

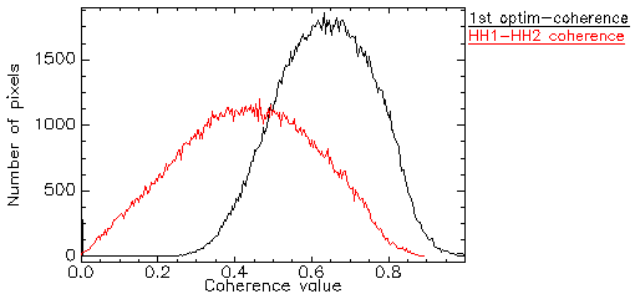

Figure 3. 1st optimised coherence, b) HH1-HH2 coherence

(7) and (8) contain two 3x3 complex eigenvector equations, which consequently yield three singular values $\nu(\nu_1, \nu_2, \nu_3)$ with $\nu_1 \geq \nu_2 \geq \nu_3 \geq 0$ and three pairs (one for each image) of eigenvectors $\{\overrightarrow{\omega_{1i}}, \overrightarrow{\omega_{2i}}\}$, with i=1,2,3 representing the optimum scattering mechanisms. The projection of the scattering vectors $\overrightarrow{k_1}$ and $\overrightarrow{k_2}$ onto $\overrightarrow{\omega_{1i}}$ and $\overrightarrow{\omega_{2i}}$ leads to the two optimized scalar complex images i_1 and i_2, which are used for the interferogram formation.

$$i_1 i_2^* = \left(\overrightarrow{\omega_{1i}}^{*T}\overrightarrow{k_1}\right)\left(\overrightarrow{\omega_{2i}}^{*T}\overrightarrow{k_2}\right)^{*T} = \overrightarrow{\omega_{1i}}^{*T}[\Omega_{12}]\overrightarrow{\omega_{2i}} \qquad (9)$$

The maximum coherence value is given by:

$$\gamma = \sqrt{\nu} \quad \Rightarrow \quad \gamma_{max} = \sqrt{\nu_{max}} \qquad (10)$$

Where ν_{max} is tha maximum eigenvalue.

With γ_{max} we obtain $\overrightarrow{\omega_{1opt}}$ and $\overrightarrow{\omega_{2opt}}$ as the corresponding eigenvectors. These are the optimum scattering mechanisms. An interferogram can be formed from the optimized scalar complex images i_{1opt} and i_{2opt} :

$$i_{1opt} i_{2opt}^* = \overrightarrow{\omega_{1opt}}^{*T}[\Omega_{12}]\overrightarrow{\omega_{2opt}} \qquad (11)$$

Comparing the 1st optimized coherence with the linear coherence HH1-HH2 by using their corresponding histograms shown in Fig. 3, we note that the potential improvement that this technique provides in the generation of an optimum coherence is observed. The derived statistical, confirms the effectiveness of this approach. The 1st optimized coherence has a maximum value of 0.99 with a mean value of 0.64 and standard deviation of 0.13 contrary to the second classical coherence which has has a maximum value of 0.89 with a mean value of 0.43 and standard deviation of 0.18.

The template is used to format your paper and style the text. All margins, column widths, line spaces, and text fonts are prescribed; please do not alter them. You may note peculiarities. For example, the head margin in this template measures proportionately more than is customary. This measurement and others are deliberate, using specifications that anticipate your paper as one part of the entire proceedings, and not as an independent document. Please do not revise any of the current designations.

III. Prepare Your Paper Before Styling

Before you begin to format your paper, first write and save the content as a separate text file. Keep your text and graphic files separate until after the text has been formatted and styled. Do not use hard tabs, and limit use of hard returns to only one return at the end of a paragraph. Do not add any kind of pagination anywhere in the paper. Do not number text heads-the template will do that for you.

Finally, complete content and organizational editing before formatting. Please take note of the following items when proofreading spelling and grammar:

A. *Abbreviations and Acronyms*

Define abbreviations and acronyms the first time they are used in the text, even after they have been defined in the abstract. Abbreviations such as IEEE, SI, MKS, CGS, sc, dc, and rms do not have to be defined. Do not use abbreviations in the title or heads unless they are unavoidable.

IV. Optimization using the Polarimetric Signatures

The interferograms can be formed by using not only linear polarization states but also any other combination between arbitrary elliptical polarization states. All elliptical polarization states can be generated by applying a change of polarization basis to transform the scattering vector (expressed in the (H,V) basis) into another scattering vector expressed in any other orthogonal basis (X,Y) as explained. The corresponding transformation of the scattering lexicographic polarimetric vector $\overrightarrow{k_l}$ in the new basis is [8]:

$$\overrightarrow{k_l'} = [U_3]\overrightarrow{k_l} \qquad (12)$$

Where U_3 is the transformation matrix given as:

$$[U_3] = \frac{1}{2}\begin{bmatrix} a+b-jcd & \sqrt{2}(c+jad) & b-a+jcd \\ jd-cb & \sqrt{2}ab & d-a-jcb \\ jd+cb & \sqrt{2}(-c+jad) & b+a+jcd \end{bmatrix} \qquad (13)$$

With $a = cos(2\psi)$, $b = cos(2\chi)$, $c = sin(2\psi)$, and $d = sin(2\chi)$

To determine (χ, ψ), a processing algorithm has been developed to accurately and efficiently measure the location of the global maximum of the radar cross section $\sigma(\chi, \psi)$ of a copolarization signature in (χ, ψ) space as mentioned by Fig. 4. $\sigma(\chi, \psi)$ is computed and represented graphically by calculating the transmit and the receive Stokes vectors ($\vec{g}_t$ and $\overrightarrow{g_r}$ respectively)and the Kennaugh matrix $[K]$. This later is a 4x4 symmetrical matrix calculated from the coherency matrix. The backscattering radar cross section is given by [9]:

$$\sigma(\chi, \psi) = \overrightarrow{g_r}[K]\vec{g}_t^T \qquad (14)$$

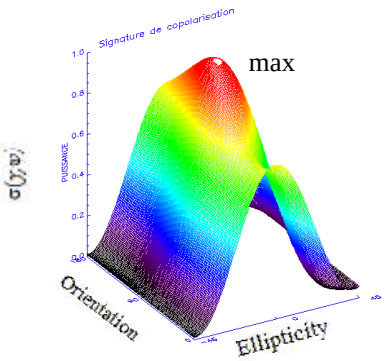

Figure 4. Co-polarimetric signature

The subscripts r and t denote the received and the transmitted polarizations. k is the transmitted wavenumber, ψ and χ are the orientation and the ellipticity angles. The first angle (ψ) ranges between 0° to 180° and the second one (χ) is defined between -45° to 45°. The Stokes vector is defined as:

$$\vec{g} = [1 \quad \cos(2\psi)\cos(2\chi) \quad \sin(2\psi)\cos(2\chi) \quad \sin(2\chi)]^T \quad (15)$$

This global maximum algorithm does a direct search over (χ, ψ)space for the maximum of signature. In the algorithm, the location of the maximum is determined for each resolution cell (image pixel). The ellipticity and orientation angles (χ, ψ) corresponding to the maximum of the polarimetric signature are extracted to measure the interferometric matrix and phases.

The possibility of transforming the scattering vector into any orthogonal polarimetric basis allows us to form interferograms between all possible elliptical polarization states. After transforming both scattering vectors $\overrightarrow{k_{l1}}$ and $\overrightarrow{k_{l2}}$ from the $\{h, v\}$ basis we obtain the matrices corresponding to the new basis as follows:

$$[C_{11}]_{(\chi,\psi)} = \langle [U_3]\overrightarrow{k_{l1}}\overrightarrow{k_{l1}}^{*T}[U_3]^{*T}\rangle = \langle [U_3][C_{11}][U_3]^{*T}\rangle \quad (16)$$

$$[C_{22}]_{(\chi,\psi)} = \langle [U_3]\overrightarrow{k_{l2}}\overrightarrow{k_{l2}}^{*T}[U_3]^{*T}\rangle = \langle [U_3][C_{22}][U_3]^{*T}\rangle \quad (17)$$

$$[\Omega_{12}]_{(\chi,\psi)} = \langle [U_3]\overrightarrow{k_{l1}}\overrightarrow{k_{l2}}^{*T}[U_3]^{*T}\rangle = \langle [U_3][\Omega_{12}][U_3]^{*T}\rangle \quad (18)$$

A new interferometric matrix $[\gamma]$ can be then defined as:

$$[\gamma]_{(\chi,\psi)} = [\Omega_{12}]_{(\chi,\psi)} ./ \sqrt{[C_{11}]_{(\chi,\psi)} .* [C_{22}]_{(\chi,\psi)}} \quad (19)$$

Which are

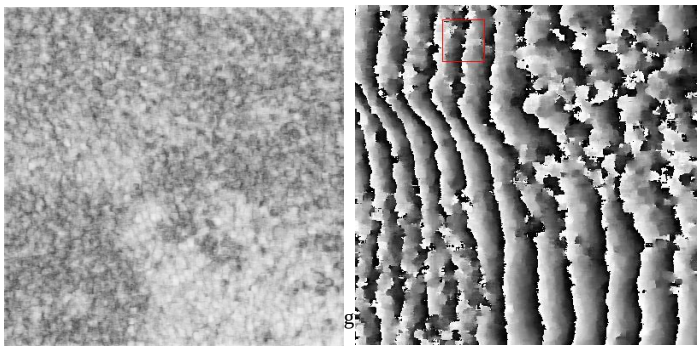

(a) (b)

Figure 6. (a) Coherence and (b) Interferogram

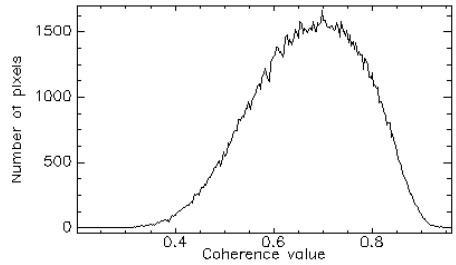

Figure 7. Coherence histogram

$$[\gamma]_{(\chi,\psi)} = \begin{bmatrix} \gamma_{xx-xx} & \gamma_{xx-xy} & \gamma_{xx-yy} \\ \gamma_{xy-xx} & \gamma_{xy-xy} & \gamma_{xy-yy} \\ \gamma_{yy-xx} & \gamma_{yy-xy} & \gamma_{yy-yy} \end{bmatrix} \quad (20)$$

Where x and y denote two arbitrary elliptical polarizations.

The resulting interferometric phases are given by:

$$[\phi]_{int} = \arg([\gamma]_{(\chi,\psi)}) \quad (21)$$

The best interferometric phase estimate will be obtained by selecting the combination that maximizes the coherence between different polarization states in $[\gamma]_{(\chi,\psi)}$. The resulted coherence, its histigoram and the corresponding interferogram are shown in Fig. 5 and Fig. 6 respectively. The basic statistics of the resulted coherence image indicate that this coherence has a maximum of 0.96, a mean of 0.67 and a standard deviation of 0.10. Comparing these results with the HH1-HH2 and the optimized coherences, we note that the coherence obtained with the second approach which is the polarimetric algorithm based on the eigenvalue problem is higher than that obtained by selecting the polarization state that maximizes the coherence as indicated by the histograms shown in Fig. 7. Again, the PS-coherence is better than the classical because of its high max and mean values and its low standard deviation as represented in Table 1. These observations are confirmed by the circles.

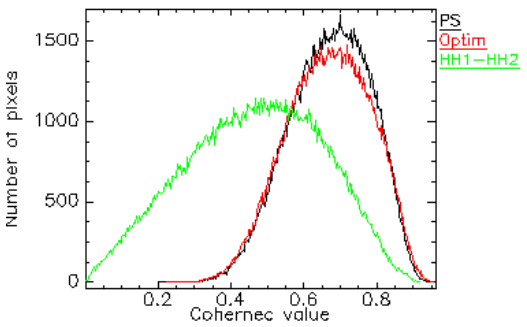

Figure 8. The three coherence histograms of the 1st optimum, PS and HH1-HH2

TABLE I. BASIC STATISTICS OF THE 1ST OPTIMIZED AND THE HH1-HH2 COHERENCES

Basic Stats	Min	Max	Mean	Stdev
PS-Coherence	0.00	0.96	0.67	0.10
1st optim-coherence	0.00	0.99	0.64	0.13
HH1-HH2 coherence	0.00	0.89	0.43	0.18

V. CONCLUSION

The aim of this paper was to investigate whether the polarimetry can be utilised to get better DTM (Digital Terrain Model) combined to InSAR. To this end the first task was to generate an interferogram from a couple of co-registered SLC radar images acquired in a singular polarization. The second task was to study the potential of polarimetric InSAR in the improvement of the interferogram compared to the first part, which is the conventional InSAR. As a consequence, a general formulation has been derived for coherent interferometry using polarized waves. Based on this formulation, we have solved the coherence optimization problem to obtain the three optimum scattering mechanisms that lead to the best phase estimates. Comparison with conventional single polarization estimates illustrates the significant processing gains that are possible if we have access to full polarimetric interferometric data. In this way we are able to generate interferograms related to certain independent scattering mechanisms and extract the height differences between them. Based on the resemblance assumption of the two scattering mechanisms ($\gamma_{pol} = 1$), the interferogram can be improved. Another coherence optimization method, which has been also developed and tested using the polarimetric signatures. By selecting the polarization basis for maximum copollarization in both images, the resulte interferogram exhibits an improved coherence compared to the 1st optimized coherence d

.

REFERENCE

[1] W.-M. Boerner "Recent advances in extra-wide-band polarimetry, interferometry and polarimetric interferometry in synthetic aperture remote sensing and its applications," *IEE Proc.-Rudur Sonur Nuvig.*, vol. 150, pp. 113-124, June 2003.

[2] J. O. Hagberg, L. M. H. Ulander, and J. I. H. Askne, "Repeat-pass SAR interferometry over forested terrain", *IEEE Trans. Geosci. Remote Sens*, vol. 33, Mar. 1995, pp. 331-340.

[3] K. P. Papathanassiou and S.R Cloude, "Polarimetric SAR interferometry", *IEEE Trans. Geosci. Remote Sens*, vol. 36, Sep. 1998, pp. 1551-1565.

[4] S. Guillasso. Complémentarité polarimétrie / interférométrie pour la détection et la caractérisation de cibles. *Thèse de doctorat*. Traitement du signal et télécommunication. université de Rennes1, France, Novembre 2003.

[5] M.Ouarzeddine, B. Souissi, A. Belhadj-Aissa. Amélioration de la cohérence interférométrique par utilisation de la polarimétrie InSAR. Revue de Télédétection de l'AUF. Volume 8, Septembre 2008.

[6] V. Alberga, "Comparison of polarimetric methods in image classification and SAR interferometry application ," PhD thesis, Institut fur Hochfrequenztechnik und Radarsysteme Oberpfaffenhofen, Germany, May 2005.

[7] F. H., Ramon, Radar interferometry: data interpretation and error analysis, *Kluwer academic publishers*, New York, 2002.

[8] L. Sagués, J. M. Lopez-Sanchez, J. Fortuny, X. Fàbregas, A. Broquetas, and A. J. Sieber, "Indoor expirement on Polarimetric SAR interferometry," *IEEE Trans. Geosci. Remote Sens* , vol. 38, Mar.2000, pp. 475-489.

[9] F. T. Ulaby and C. Elachi, "Radar polarimetry for geoscience applications," *Artech House*, Norwood, MA, 1990

.